AGU PUBLICATIONS

Water Resources Research

RESEARCH ARTICLE
10.1002/2015WR017755

Key Points:
- SE Asian rubber plantations maintain very high annual evapotranspiration (ET)
- Access to deep soil water enables rapid refoliation after leaf drop and high late dry season ET
- Spatially rubber evapotranspiration increases linearly with increasing net radiation

Supporting Information:
- Supporting Information S1

Correspondence to:
T. Giambelluca,
thomas@hawaii.edu

Citation:
Giambelluca, T. W., et al. (2016), Evapotranspiration of rubber (*Hevea brasiliensis*) cultivated at two plantation sites in Southeast Asia, *Water Resour. Res.*, *52*, 660–679, doi:10.1002/2015WR017755.

Received 9 JUL 2015
Accepted 7 JAN 2016
Accepted article online 12 JAN 2016
Published online 4 FEB 2016

Evapotranspiration of rubber (*Hevea brasiliensis*) cultivated at two plantation sites in Southeast Asia

Thomas W. Giambelluca[1,2], Ryan G. Mudd[1], Wen Liu[1], Alan D. Ziegler[3], Nakako Kobayashi[2], Tomo'omi Kumagai[2], Yoshiyuki Miyazawa[1,4], Tiva Khan Lim[5], Maoyi Huang[6], Jefferson Fox[7], Song Yin[5], Sophea Veasna Mak[5], and Poonpipope Kasemsap[8]

[1]Department of Geography, University of Hawai'i at Mānoa, Honolulu, Hawai'i, USA, [2]Hydrospheric Atmospheric Research Center, Nagoya University, Nagoya, Japan, [3]Department of Geography, National University of Singapore, Singapore, Singapore, [4]Research Institute of East Asia Environments, Kyushu University, Fukuoka, Japan, [5]Cambodian Rubber Research Institute, Phnom Penh, Cambodia, [6]Atmospheric Sciences and Global Change Division, Pacific Northwest National Laboratory, Richland, Washington, USA, [7]East-West Center, Honolulu, Hawai'i, USA, [8]Department of Horticulture, Kasetsart University, Bangkok, Thailand

Abstract To investigate the effects of expanding rubber (*Hevea brasiliensis*) cultivation on water cycling in Mainland Southeast Asia (MSEA), evapotranspiration (*ET*) was measured within rubber plantations at Bueng Kan, Thailand, and Kampong Cham, Cambodia. After energy closure adjustment, mean annual rubber *ET* was 1211 and 1459 mm yr^{-1} at the Thailand and Cambodia sites, respectively, higher than that of other tree-dominated land covers in the region, including tropical seasonal forest (812–1140 mm yr^{-1}), and savanna (538–1060 mm yr^{-1}). The mean proportion of net radiation used for *ET* by rubber (0.725) is similar to that of tropical rainforest (0.729) and much higher than that of tropical seasonal forest (0.595) and savanna (0.548). Plant area index (varies with leaf area changes), explains 88.2% and 73.1% of the variance in the ratio of latent energy flux (energy equivalent of *ET*) to potential latent energy flux (LE/LE_{pot}) for mid-day rain-free periods at the Thailand and Cambodia sites, respectively. High annual rubber *ET* results from high late dry season water use, associated with rapid refoliation by this brevideciduous species, facilitated by tapping of deep soil water, and by very high wet season ET, a characteristic of deciduous trees. Spatially, mean annual rubber *ET* increases strongly with increasing net radiation (R_n) across the three available rubber plantation observation sites, unlike nonrubber tropical ecosystems, which reduce canopy conductance at high R_n sites. High water use by rubber raises concerns about potential effects of continued expansion of tree plantations on water and food security in MSEA.

1. Introduction

The influence of land cover change, especially deforestation, on water flows is one of the most important and longstanding topics of hydrological research [*Hoover*, 1944; *Hibbert*, 1965; *Bosch and Hewlett*, 1982; *Bruijnzeel*, 2004]. Decades of observations and model simulations have shown that forests generally support high evapotranspiration (*ET*) and produce lower annual stream discharge than other land covers, but might enhance dry season flows [*Brown et al*., 2013; *Beck et al*., 2013]. Globally, land cover change, dominated by conversion of natural vegetation to cropland, has led to increased runoff, partly as a result of reduced *ET* [*Sterling et al*., 2013]. In recent years, however, reforestation for a variety of purposes has led to a slowdown in the loss of tree cover and even a reversal in some regions [*Meyfroidt and Lambin*, 2011]. While numerous perceived benefits are associated with tree planting [*Malmer et al*., 2010], negative effects of increased tree cover on water resources have been observed. For example, expansion of tree plantations in Australian catchments resulted in streamflow reductions, especially for ephemeral streams, leading to a greater number of zero-flow days [*Zhang et al*., 2012]. However, the possible effects of expanding tree cover on water resources are not always clear [*van Dijk and Keenan*, 2007], especially in the tropics, where estimates are often extrapolated from extratropical data [*Malmer et al*., 2010] because of the paucity of tropical research results [*Wohl et al*., 2012].

As in other areas in the developing tropics, land cover change in Mainland Southeast Asia (MSEA), including Thailand, peninsular Malaysia, Cambodia, Laos, Myanmar, and the southern part of Yunnan, China, had until

recent decades been dominated by activities associated with forest clearing, especially logging and shifting agriculture [*Fox et al*., 1995]. In the last few decades, subsistence cultivation has given way in many areas to commercial agriculture [*Fox*, 2012], often in the form of tree plantations such as rubber [*Li and Fox*, 2011; *Ziegler et al*., 2009a, 2009b, 2011; *Mann*, 2009; *Manivong and Cramb*, 2008], fruit and nut orchards, oil palm, and paper pulp species, and reforestation for conservation and carbon storage [*Fox et al*., 2014]. Commercial tree plantations are already displacing forests, and much of the projected expansion of rubber cultivation is likely to be at the expense of forests, including protected areas [*Warren-Thomas et al*., 2015]. Rubber cultivation is currently leading the expansion of tree plantations in MSEA [*Li and Fox*, 2011; *Fox and Castella*, 2013], driven by spiraling global demand for rubber and the consequent 10-fold increase in the market price of natural rubber latex over the 10 year period ending in February 2011 (www.indexmundi.com/commodities, accessed 20 June 2015). While commodity prices can fluctuate (May 2015 rubber price was 70% below its February 2011 peak), expansion of rubber cultivation over the past decade has been explosive, and rubber is likely to continue to be one of the fastest growing land cover types in MSEA over the coming decades due to projected increases in demand [*Warren-Thomas et al*., 2015]. The locus of new rubber plantations represents a northward and in some cases upward shift from the traditional rubber growing areas of lowland Malaysia and southern Thailand into areas throughout the region with more seasonal rainfall regimes and lower annual minimum temperatures. With the development of rubber clones appropriate for higher latitude/elevation environments such as Xishuangbanna, a district along the southern border of Yunnan, China, a new "non-traditional" rubber cultivation region began to emerge [*Ziegler et al*., 2009a]. In recent decades, the extent of rubber cultivation in nontraditional rubber growing areas of MSEA has increased by more than a million hectares [*Ziegler et al*., 2009a; *Qiu*, 2009].

The unbridled expansion of rubber in some areas is raising concerns about impacts on biodiversity [*Li et al*., 2007] and ecosystem services [*Hu et al*., 2008], including water cycling [*Guardiola-Claramonte et al*., 2008; *Ziegler et al*., 2009a] and carbon storage [*Li et al*., 2008; *Ziegler et al*., 2012; *Fox et al*., 2014]. *Tan et al*. [2011] called rubber plantations in Xishuangbanna "water pumps" because of their high *ET* rates compared with natural forest. *Guardiola-Claramonte et al*. [2008] found high rates of root-water extraction during the mid to late dry season under rubber as compared with other vegetation in Xishuangbanna. Their findings suggest that the high annual *ET* of rubber might be explained by species-specific biological control enabling high water use in the dry season. However, estimates of rubber transpiration based on sap flow measurements have not found unusually high water use rates [*Isarangkool Na Ayutthaya et al*., 2011; *Kobayashi et al*., 2014].

Our research is motivated by the concern that if rubber does maintain high annual *ET* rates as found by *Tan et al*. [2011] and as suggested by the findings of *Guardiola-Claramonte et al*. [2010], the replacement of native and other nonrubber vegetation by rubber in MSEA may have significant negative consequences for water resources in the region. To improve understanding of the potential impacts of expanding rubber cultivation on water fluxes, the objectives of this study were to: (1) determine annual *ET* of rubber plantations at representative sites in MSEA, in order to compare *ET* of rubber plantations with those of other tree-dominated land covers to assess whether rubber is exceptional in its water use traits; (2) determine the roles of phenological and environmental controls on the annual cycle of *ET* and elucidate the mechanisms promoting high annual *ET*; and (3) evaluate the environmental controls that give rise to spatial differences in rubber *ET* in MSEA. To address these objectives, field research stations were established in two rubber plantations in the region. Eddy covariance and related measurements were made at each site beginning in 2009. Herein, we report results from approximately two years of measurements at each site.

2. Methods

2.1. Study Sites

Observations were conducted at two monoculture rubber plantation stands in mainland SE Asia; Som Sanuk, Bueng Kan Province, NE Thailand beginning in February 2009, and the Cambodian Rubber Research Institute (CRRI) plantation in Kampong Cham Province, central Cambodia beginning in September 2009. Study site characteristics are given in Table 1. Herein, we present *ET* estimates for March 2009 to June 2011 at Som Sanuk and for late September 2009 to January 2012 at CRRI. Annual values are given for two years at each site: March 2009 to February 2011 at Som Sanuk and calendar years 2010–2011 at CRRI. Data

Table 1. Study Site Characteristics

Characteristic	Som Sanuk, Thailand	CRRI, Cambodia
Coordinates	18°12′N, 103°25′E	11°57′N, 105°34′E
Elevation (m)	210	57
Terrain	Slightly undulating	Very gently sloping
Average slope (°)	<1	<1
Year planted	1991	2004
Tower height (m)	26.5	30.0
Fetch (m)	>500	>500
Clone	RRIM-600	RRIC-100
Spacing (m)	7 × 2.5	6 × 3
Planted tree density (trees ha^{-1})	567	555
Tree density at start of obs. (trees ha^{-1})	525	431
Mean canopy height at start of obs. (m)	19.0	11.4[a]
Mean stem diameter at 1.7 m (cm)	18.9 ± 3.0	13.3 ± 2.3
Mean stem diameter growth rate (cm yr^{-1})	0.6	1.8
Understory	Sparse	Abundant
Tapping initiation date	1997	Nov 2010
Tapping interval (tapping days|rest days)	2|1	1|2
Fertilizer application frequency (yr^{-1})	2	2[b]
Fertilizer type	50/50 manure & N-P-K: 20-10-12	N-P-K: 15-15-15
Herbicide use	None	Annual
Dry season	Oct–Apr	Nov–Apr
Wet season	May–Sep	May–Oct
Cool season	Nov–Jan	Nov–Jan
Annual rainfall – project year 1 (mm)	2215	1332
Annual rainfall – project year 2 (mm)	2020	1545
Mean ann. temperature – project yr 1 (°C)	26.2	28.0
Mean ann. temperature – project yr 2 (°C)	26.0	27.0
Wind - dry season (dom. direction|freq.)	NE (57%)	NE (72%)
Wind - wet season (dom. direction|freq.)	SW (42%)	S (82%)

[a]Increased from this height in February 2010 to 12.9 m in March 2011.
[b]Applied during first 4 years after planting only.

presented for leaf area extend to December 2012 at Som Sanuk and September 2013 at CRRI to allow better understanding of the annual leaf area cycle. See supporting information Text S1 for more details on the study sites.

2.2. Instrumentation and Data Analysis

2.2.1. Eddy Covariance Variables

Latent energy flux (*LE*) and sensible energy flux (*H*) were estimated via the eddy covariance (EC) technique. A three-dimensional sonic anemometer (CSAT3, Campbell Scientific, Logan, UT, USA) and an open-path infrared gas analyzer (IRGA, model LI-7500, LiCor, Lincoln, NE, USA) were mounted to the meteorological towers at 26.5 and 30.1 m above the ground, at Som Sanuk and CRRI, respectively. The orientation of the CSAT3 and LI-7500 sensors were changed seasonally toward the prevailing wind direction (southwest in wet season, north in dry season) to limit turbulence effects caused by the tower structure. The 10 Hz eddy covariance measurements were stored using a Campbell Scientific CR3000 data logger for post processing, and all other variables (see below) were stored at a 30 min interval using a Campbell Scientific CR23X data logger. The code to process the EC data was adapted from that of *Noormets et al.* [2007] and *Baldocchi et al.* [1988] [also see *Giambelluca et al.*, 2009a]. Details of the flux calculations are given in supporting information Text S2.

The 30 min fluxes were filtered using the LI-7500 output diagnostic index (*AGC*) that responds to the presence of water droplets on sensor windows. The flux data were also filtered for gross energy balance anomalies (*EBA*). We defined the variable $EBA = R_n - G - LE - H$, where G is soil heat flux. Fluxes estimates were excluded for any 30 min period for which $EBA < -200$ or $EBA > 400$ W m^{-2}. Tower interference was evaluated and determined to be negligible (see supporting information Text S3).

2.2.2. Meteorological Variables

Time series of 30 min rainfall, net radiation (R_n), air temperature (T_a), relative humidity (*RH*), wind speed (*WS*), and wind direction (*WD*) were also measured. See supporting information Text S4.

2.2.3. Soil Moisture

At Som Sanuk, soil moisture was measured using six water content reflectometers (CS616, Campbell Scientific) placed in the soil profile at the following depths and orientations: 0.04 m horizontal, 0.04–0.34 m vertical, 0.48–0.75 m vertical, 0.80 m horizontal, 1.50–1.80 m vertical, and 2.20–2.50 m vertical. At CRRI, soil moisture was measured using five CS616s placed in the soil profile at: 0.04 m horizontal, 0.35–0.65 m vertical, 1.05–1.35 m vertical, 2.03–2.33 m vertical, and 3.08–3.38 m vertical. In addition, five ML2X ThetaProbe

(Delta-T Devices, Burwell, UK) soil moisture sensors were installed horizontally at depths of 0.05, 0.10, 0.20, 0.30, and 0.50 m. The time series of integrated profile soil moisture at each site was obtained by assigning depth ranges to each sensor, with the boundaries of each layer delineated at the midpoint between successive sensors.

2.2.4. Plant Area Index

Plant area index (*PAI*, $m^3\ m^{-3}$) estimates were obtained using a plant canopy analyzer (LAI-2000 or LAI 2200, Li-Cor, Lincoln, NE) at both sites at irregular time intervals over the course of the study. Note that the lowest rings of the LAI-2000 and LAI-2200 were masked to minimize the contributions of tree stems and branches. Emphasis was placed on sampling *PAI* frequently during leaf shedding and flushing periods, and periodically throughout the year to approximate the annual cycle of foliage accumulation and loss throughout the study period. Data were collected at a height of approximately 1.2 m above the ground and at 6 m intervals at Som Sanuk and 5 m intervals at CRRI along transects oriented diagonally with respect to tree rows; the interval was selected as 1 m less than the row separation, which with the diagonal transect, resulted in even sampling across the planting rows. In addition, at Som Sanuk only, daily *PAI* was estimated based on measurements of photosynthetically active radiation above (PAR_A) and below (at 2 m above the ground) the canopy (PAR_B). PAR_A was estimated using the relationship between solar radiation (CNR1, Kipp, and Zonen) and PAR (LI-190, LI-COR, Lincoln NE) for the period when the PAR sensor was less than 1 month old, before significant calibration drift occurred. PAR_B was measured with a line quantum sensor (model SQ-321, Apogee Instruments, Logan, UT, USA). In homogeneous vegetation, *PAI* can be estimated using a relationship derived from the Beer-Lambert Law [*Monsi and Saeki*, 1953, 2005; *Law and Waring*, 1994]:

$$PAI = -\frac{\ln\left(\frac{PAR_B}{PAR_A}\right)}{k} \tag{1}$$

where the extinction coefficient $k = G/cos(\beta)$, G is the leaf inclination distribution function, defined as the cosine of the angle between the solar zenith and the normal to the mean leaf orientation, and β is the solar zenith angle. To mitigate foliar clumping effects [*Ryu et al*., 2010], only periods when the solar zenith angle was near one radian were used. Thus, for each day, one morning and one afternoon sample were averaged. Because *PAI* estimates derived from this method are affected by variations in diffuse light content due to cloud cover, wet season values are considered to be more uncertain than dry season values. Note that *PAI* measurements exclude understory vegetation, which was very sparse at Som Sanuk and substantial at CRRI (see supporting information Figure S1).

To develop a continuous time series of *PAI* at each site, points between measurements were estimated based on LAI2000 and LAI2200 measurements for the same time of year in previous or later years, variations in albedo, *PAI* estimates derived from the ratio of below to above-canopy PAR measurements (at Som Sanuk only), and visual observations; the time series lines were smoothed using a cubic spline.

2.2.5. Soil Heat Flux

The 30 min time series of soil heat storage (G, $W\ m^{-2}$) was calculated from the output of four plates (model HFP01, Hukseflux) placed at a depth of 0.08 m, the averaged soil temperatures (T_{soil}, K) of two 4-probe sensors (model TCAV, Campbell Scientific) installed at depths of 0.02 and 0.06 m, and the volumetric soil moisture of one horizontally oriented reflectometer (CS-616, Campbell Scientific) at a depth of 0.04 m. The variable G represents the sum of soil heat flux at 0.08 m (F) and heat storage in the 0.08 m soil layer above the heat flux plates (M), which are given as:

$$G = F + M \tag{2}$$

$$F = \frac{SHF_1 + SHF_2 + SHF_3 + SHF_4}{4} \tag{3}$$

$$M = \frac{dT_{soil}}{dt} D(\rho_b C_s + \rho_w \theta C_w) \tag{4}$$

where SHF_j is the soil heat flux ($W\ m^{-2}$) measured at 0.08 m depth by sensor j, dT_{soil} is the change in temperature in the upper 0.08 m soil layer (K) during the time interval dt (1800 s), D is the depth of soil heat flux plates (0.08 m), ρ_b is site-specific soil bulk density of the upper 0.08 m of soil ($kg\ m^{-3}$), C_S is the specific heat for mineral soil ($840\ J\ kg^{-1}\ K^{-1}$), ρ_w is the density of water (approximated as $1000\ kg\ m^{-3}$), θ is the volumetric soil moisture content of the upper 0.08 m soil layer, assumed equal to the 0.04 m horizontal soil moisture

sensor value ($m^3\ m^{-3}$), and C_W is the specific heat of water (4186 J $kg^{-1}\ K^{-1}$). Site-specific ρ_b was determined to be 1295 kg m^{-3} at Som Sanuk and 1138 kg m^{-3} at CRRI, based on the average oven-dry mass of eight and six samples of known volume at Som Sanuk and CRRI, respectively.

2.2.6. Biomass and Air Layer Heat Storage

The 30 min time series of sensible heat storage in the biomass is a function of temporal change in temperature, mass, and specific heat of each major component of the above ground biomass of the rubber trees:

$$S_{bio} = \sum \frac{dT_{bio\_i}}{dt}(C_i BM_i) \tag{5}$$

where S_{bio} is the change in sensible heat stored in the biomass per unit ground area (W m^{-2}), i indicates the different components of the aboveground biomass (main stems, branches, and leaves), dT_{bio_i} is the change in temperature of biomass component i (K) during the time interval, dt (1800 s), C_i is the specific heat of biomass component i (J $kg^{-1}\ K^{-1}$); and BM_i is the fresh biomass (including water content) of component i (kg m^{-2}). Details of the biomass energy storage estimates are given in supporting information Text S5.

The change in stored energy in the air layer under the EC sensors (S_{air}; W m^{-2}) was estimated, including changes in stored sensible and latent heat (S_{air_h} and S_{air_LE}, respectively). S_{air_h} was estimated from field measurements of T_a using shielded thermocouples at heights of 3, 9, and 15 m on the tower at Som Sanuk; and at heights of 3, 5, and 7 m on the tower at CRRI, and the temperature sensors (HMP45C) at the top of each tower. No humidity measurements were made within the canopy; therefore, the top-of-tower HMP45C humidity time series was used as an approximation. For each 30 min period, the change in stored energy was estimated as

$$S_{air} = S_{air\_h} + S_{air\_LE} \tag{6}$$

$$S_{air\_h} = z\frac{dT_a}{dt}\left[\left(C_p \rho_{dry\_air}\right) + \left(C_{wv} q\right)\right] \tag{7}$$

$$S_{air\_LE} = z\frac{dq}{dt}\lambda \tag{8}$$

where z is the depth of the air layer (27 m at Som Sanuk and 30.1 m at CRRI), dT_a is change in mean air layer temperature (K) during the time interval dt (1800 s), C_p is specific heat of dry air at constant pressure (1004 J $kg^{-1}\ K^{-1}$), ρ_{dry_air} is the dry air density (kg m^{-3}), C_{wv} is the specific heat of water vapor (J $kg^{-1}\ K^{-1}$), q is the water vapor density (kg m^{-3}), and λ is the latent heat of vaporization (J kg^{-1}), estimated as a function of air temperature.

2.2.7. Gap Filling

Data gaps created by missing observations and filtering of data during quality control procedures, e.g., removal of poor quality data associated with wet sensor conditions, lead to problems in data analysis and aggregation. For example, because of the pronounced diurnal cycle in most variables, averaging the remaining values in a time series with many gaps can produce severely biased results. Therefore, it is preferable to implement gap-filling techniques, in which missing values are replaced with estimates to produce a time series as close to serially complete as possible [*Falge et al.*, 2001]. The 30 min time series of *LE* and *H* flux for each site were gap-filled using regressions of each flux variable with available energy ($A = R_n - G - S_{bio} - S_{air}$). Initially, one regression was performed for each month of the year, combining data for the same month in different years. Subsequently, months with very similar relationships were merged. For Som Sanuk, grouping resulted in five "seasons": January, February, March–October, November, and December. For CRRI, six separate seasons were used: January, February, March, April, May–November, and December. For all instances of a missing value of *LE* or *H*, during a time interval when *A* was available, the estimated value derived from the appropriate regression was substituted to fill the gap. This procedure increased the number of 30 min *LE* estimates from 34,249 to 37,301 at Som Sanuk, raising the proportion of data available from 83.7 to 91.2%, and from 35,228 to 37,743 at CRRI, increasing available data from 86.0 to 92.2%. Gap-filled data were used to calculate the mean of each 30 min period in each month, from which monthly means (or sums) were obtained. Monthly means were used to calculate annual values.

2.2.8. Energy Closure Adjustment

As a test of eddy covariance flux estimates, energy balance closure is commonly evaluated by comparing the sum of estimated turbulent fluxes ($LE + H$) to the available energy (A). For most eddy covariance sites,

$LE + H$ is less than A. For example, at most tropical forest flux tower sites in the Large-Scale Biosphere Atmosphere Experiment (LBA) in Amazonia, energy closure error was in the 20–30% range [*Fisher et al*., 2009]. While much has been written about the numerous possible sources of energy closure error [*Twine et al*., 2000; *Wilson et al*., 2002; *Fisher et al*., 2009; *Franssen et al*., 2010; *Leuning et al*., 2012], it is widely assumed that energy closure error results from underestimation of both *LE* and *H* rather than an overestimate of *A*. Further, it is sometimes assumed that despite underestimation of *LE* and *H*, the ratio of *H* to *LE* (Bowen ratio) is correctly estimated. This assumption gives rise to the use of the so-called Bowen ratio closure method recommended by *Twine et al*. [2000], in which *LE* and *H* are each adjusted by a factor of the inverse of the energy closure ratio to force energy closure. *Kochendorfer et al*. [2012] suggests that a significant source of underestimation of *LE* and *H* can be traced to a systematic bias in vertical wind speed measurements from sonic anemometers [also see *Nakai and Shimoyama*, 2012], a finding that supports the use of the Bowen ratio closure method.

Energy balance closure can be evaluated in terms of the ratio of the sum of turbulent fluxes ($LE + H$) to the available energy (A). If assessed at each 30 min time interval, this ratio is very noisy and, therefore, time averaging is needed to smooth it for use in adjusting flux data to force energy closure. At each 30 min time step (i), a centered 1000.5 h (2001 30 min intervals) moving window energy closure ratio (ECR_i) was calculated as:

$$ECR_i = \frac{\frac{\sum_{k=i-1000}^{k=i+1000} LE_k + H_k}{2001}}{\frac{\sum_{k=i-1000}^{k=i+1000} A_k}{2001}} \tag{9}$$

To achieve approximate energy closure, the values of *LE* and *H* were adjusted at each time step by a factor of ECR_i^{-1}. The results for *LE* and *H* are subsequently summarized with and without the energy closure adjustment.

2.3. Evapotranspiration Response to Environmental Demand

Variations in *ET* are driven, in part, by fluctuating environmental demand, which can be quantified in terms of potential evapotranspiration. To better understand the mechanisms controlling the response of rubber *ET* to environmental demand, as influenced by factors such as soil moisture and leaf phenology, we compared measured *ET* with potential ET at each site.

2.3.1. Analysis of Midday Rain-Free Periods

The response of rubber *ET* to variations in atmospheric demand was analyzed using a subset of data comprised of midday (09:30-14:00 local time), rain-free periods. This allowed us to focus on periods that are most strongly controlled by the physiological traits of rubber trees, i.e., mostly high solar radiation and dry-canopy conditions [see *Kumagai et al*., 2015].

2.3.2. Potential Evapotranspiration

Evaluation of variations in observed *ET* includes comparison with potential evapotranspiration derived using the Penman-Monteith equation [*Monteith*, 1965] with surface conductance set to infinity:

$$LE_{pot} = \frac{sA}{s + \gamma} + \frac{\rho_a C_p G_a VPD}{s + \gamma} \tag{10}$$

where LE_{pot} is the latent energy flux equivalent of potential *ET* (W m^{-2}), s is slope of saturation vapor pressure versus temperature curve (kPa K^{-1}), A is available energy (W m^{-2}), ρ_a is air density (kg m^{-3}), C_p is specific heat of air at constant pressure (J K^{-1} kg^{-1}), G_a is aerodynamic conductance (m s^{-1}) estimated as u_*^2/u, where u_* is the friction velocity (m s^{-1}), and u is wind speed (m s^{-1}) *VPD* is vapor pressure deficit (kPa), and γ is the psychrometric constant (kPa K^{-1}). In the form shown (equation (10)), the two terms on the right can be referred to as the energy term (LE_{pot_energy}) and the aerodynamic term ($LE_{pot\_aerodynamic}$), respectively. LE_{pot} and the two component terms were calculated for the midday rain-free periods and analyzed in comparison with observed *LE* for the same time periods.

2.3.3. Surface Conductance

By inverting the Penman-Monteith equation, surface conductance (G_s; m s^{-1}) can be calculated as:

$$G_s = \frac{G_A \gamma LE}{sA + \rho_a C_p G_a VPD - (s + \gamma) LE} \tag{10}$$

where *LE* is derived from the eddy covariance measurements. G_s was calculated for the midday rain-free periods for both sites.

2.4. Comparison with Estimates Extracted from Global *ET* Analysis

Mueller et al. [2013] mapped the global distribution of *ET* derived from a synthesis of 1985–2005 satellite-based estimates, in situ observations, and estimates from land-surface models. For the locations of our two study sites and the Xishuangbanna site [*Tan et al*., 2011], the 1989–2005 annual *ET* statistics were extracted for the relevant 1°× 1° grid cells. The mapped estimates pertain to the dominant land covers, not necessarily rubber, and therefore offer a means of evaluating *ET* of rubber in relation to that of the typical existing land covers surrounding each study site.

3. Results

3.1. Hydrometeorological Variables

The climate regimes of the two sites have similar characteristics (Figure 1). However, some differences are evident in the measured variables, reflecting the geographical contrasts in latitude and continentality. At both sites, the highly seasonal climate of the Asian Monsoon region is clearly evident in the annual cycles of rainfall, soil moisture, and VPD. The annual range of mean daily temperature is greater than 15°C at the more continental Som Sanuk site, and less than 10°C at CRRI; temperature minima are experienced early in the dry season (∼14–15 and ∼22–24°C at Som Sanuk and CRRI, respectively); maxima occur near the end of the dry season (∼31–33°C at Som Sanuk and ∼30–32°C at CRRI). With its more equatorward location, CRRI generally has higher net radiation than Som Sanuk. On relatively clear days, net radiation follows the annual course of sun angle at both sites. Cloudiness causes more day-to-day variability and attenuates average net radiation during the wet season. Monthly mean net radiation is lowest in December and January (∼100 and ∼130 W m^{-2} at Som Sanuk and CRRI, respectively) and high during April through September (∼140 W m^{-2} at Som Sanuk and ∼160 W m^{-2} at CRRI). Soil moisture variation at the two sites is responsive to the highly seasonal rainfall regime. However, while the deep layers at Som Sanuk responded rapidly to the initiation of rains marking the start of the wet season, with the wetting front reaching below 2 m depth by late May in both study years, soil moisture during 2010 remained near minimum values below 2 m depth at CRRI until late in August.

3.2. PAI

At Som Sanuk, *PAI* reached a maximum of about 5 from July to September, while the annual maximum value increased at CRRI from just over 4 in 2010 to about 4.9 in 2011, 2012, and 2013 (Figure 2). At both sites, for each year, leaf abscission significantly increased around the beginning of January. *PAI* reached a minimum in mid to late January, followed a sharp increase caused by rapid leaf flushing from around the end of January into February. Note that total *PAI* is higher at CRRI than shown in Figure 2 because of the relatively dense understory there (see supporting information Figure S1).

3.3. Energy Balance Closure

The slope and r^2 values of the regression lines for 30 min *A* versus $LE + H$ (0.84 and 0.92, respectively, at Som Sanuk, and 0.83 and 0.90, respectively, at CRRI; see supporting information Figure S2) indicate reasonably good results, well within the upper half of the range of values achieved at 22 FLUXNET sites: slope: 0.55–0.99; r^2: 0.64–0.96 [*Wilson et al*., 2002]. The ratio of mean annual $LE + H$ to mean annual *A* was 0.94 for Som Sanuk and 0.88 for CRRI. However, energy closure varied temporally at each site, with ECR_i (see equation (9)) from 0.825 to 1.025 at Som Sanuk and from 0.786 to 0.974 at CRRI. Variations in ECR_i were not strongly related to environmental variables T_a, *RH*, *WS*, *WD*, SM_z, *A*, *LE*, or *H* (max $r^2 = 0.07$ for $SM_{6\text{-}34\ cm}$ at Som Sanuk; max $r^2 = 0.04$ for T_a at CRRI).

3.4. Energy Partitioning

The monthly mean diurnal cycles of *LE* and *H* (Figure 3) illustrate the annual cycle in the relative magnitudes of the two variables, with *LE* much higher than *H* through all months except November–February at Som Sanuk and all months except December–March/April at CRRI, periods affected by dry soil and leaf shedding. The Bowen ratio (*H/LE*) remains between about 0.20 and 0.33 during May–October at Som Sanuk, then rises to a January peak of 2.27 (2010) and 3.50 (2011), before dropping rapidly to wet season values. At CRRI, the Bowen ratio is in the 0.17–0.33 range from May to December, rises to 0.80, 1.1, and 1.1 in January 2009, February 2010, and February 2011, respectively.

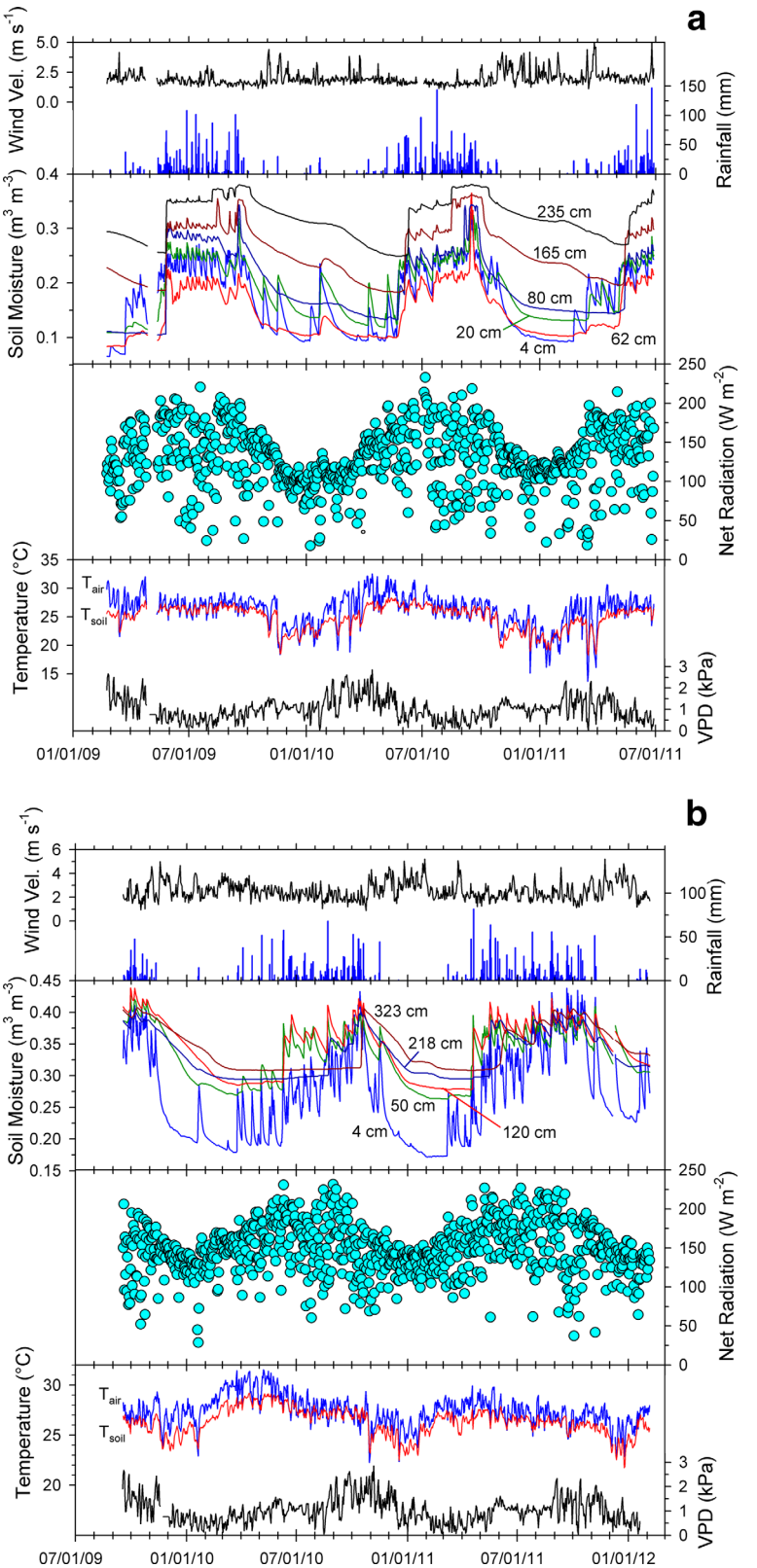

Figure 1. Daily time series of meteorological variables and soil moisture during the respective study periods at (a) Som Sanuk; and (b) CRRI.

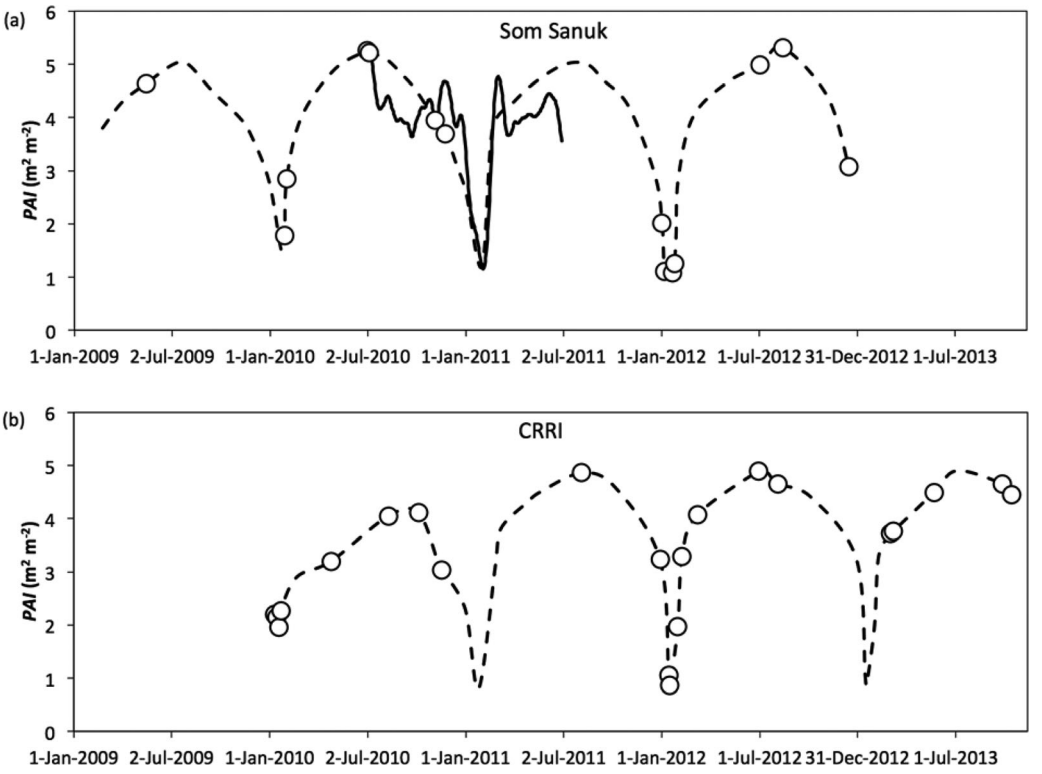

Figure 2. Leaf area Index (*PAI*) at (top) Som Sanuk and (bottom) CRRI. LAI2000 and LAI2200 measurements are shown as white circles. The solid line for Som Sanuk is the *PAI* estimate derived from the ratio of below- to above-canopy *PAR* measurements. Dashed lines represent estimated daily *PAI* based on the best available information.

3.5. Evapotranspiration

Monthly *ET* at Som Sanuk and CRRI averages 4.1 and 4.8 mm d^{-1}, respectively, during the wet season and drops to an average of 0.9 and 2.4 mm d^{-1}, respectively, during January (Figure 4). Higher January *ET* at CRRI might be explained by the denser understory at CRRI (see supporting information Figure S1). Mean annual *ET* rates based on 2 years of observations at each site are 1128 mm yr^{-1} and 1272 mm yr^{-1} for Som Sanuk and CRRI, respectively. After adjustment for energy closure, the rates are quite high at 1211 mm yr^{-1} (3.3 mm d^{-1}) and 1459 mm yr^{-1} (4.0 mm d^{-1}), respectively.

3.6. *LE* Response to Biophysical Variables

Bivariate linear regression indicates that *A* and *PAI* are the dominant controls on *LE* at the daily time scale for both sites, with *PAI* having the highest r^2 at Som Sanuk and *A* having the highest at CRRI (Table 2). *T* explains nearly half the variance in *LE* at Som Sanuk, but less than 4% at CRRI. The amount of *LE* variance explained by moisture variables, *SM* and *VPD*, is 10 and 4%, respectively, at Som Sanuk and 30 and 15%, respectively, at CRRI. The much higher responsiveness to *SM* at CRRI is likely a result of generally lower moisture availability at CRRI (mean annual precipitation is 1439 mm at CRRI and 2118 mm at Som Sanuk). *VPD* and *LE* are positively (and weakly) related at Som Sanuk, and negatively (and more strongly) related at CRRI. This suggests that, on average, the positive effect of *VPD* on evaporative demand slightly exceeds the negative effect of VPD on stomatal conductance at Som Sanuk. At CRRI, with less abundant moisture, the stomatal conductance effect is greater on average.

Correlations between environmental variables were analyzed using daily data (Table 2). Variables such as *T* and *VPD* are causally linked, while relationships between other pairs of variables may be somewhat coincidental, resulting from phase alignment of their annual cycles. Note, for example, that high correlations for *A* versus *PAI*, *A* versus *T*, and *PAI* versus *T* at Som Sanuk can be explained by the approximate coincidence of the annual cycles of these variables (see Figure 1), and do not necessarily indicate causal relationships. Hence, the strong relationship between *LE* and *T* seen in the bivariate regression results for Som Sanuk is probably a result of the high correlation between *T* and *PAI* there (0.69) compared with CRRI (0.31).

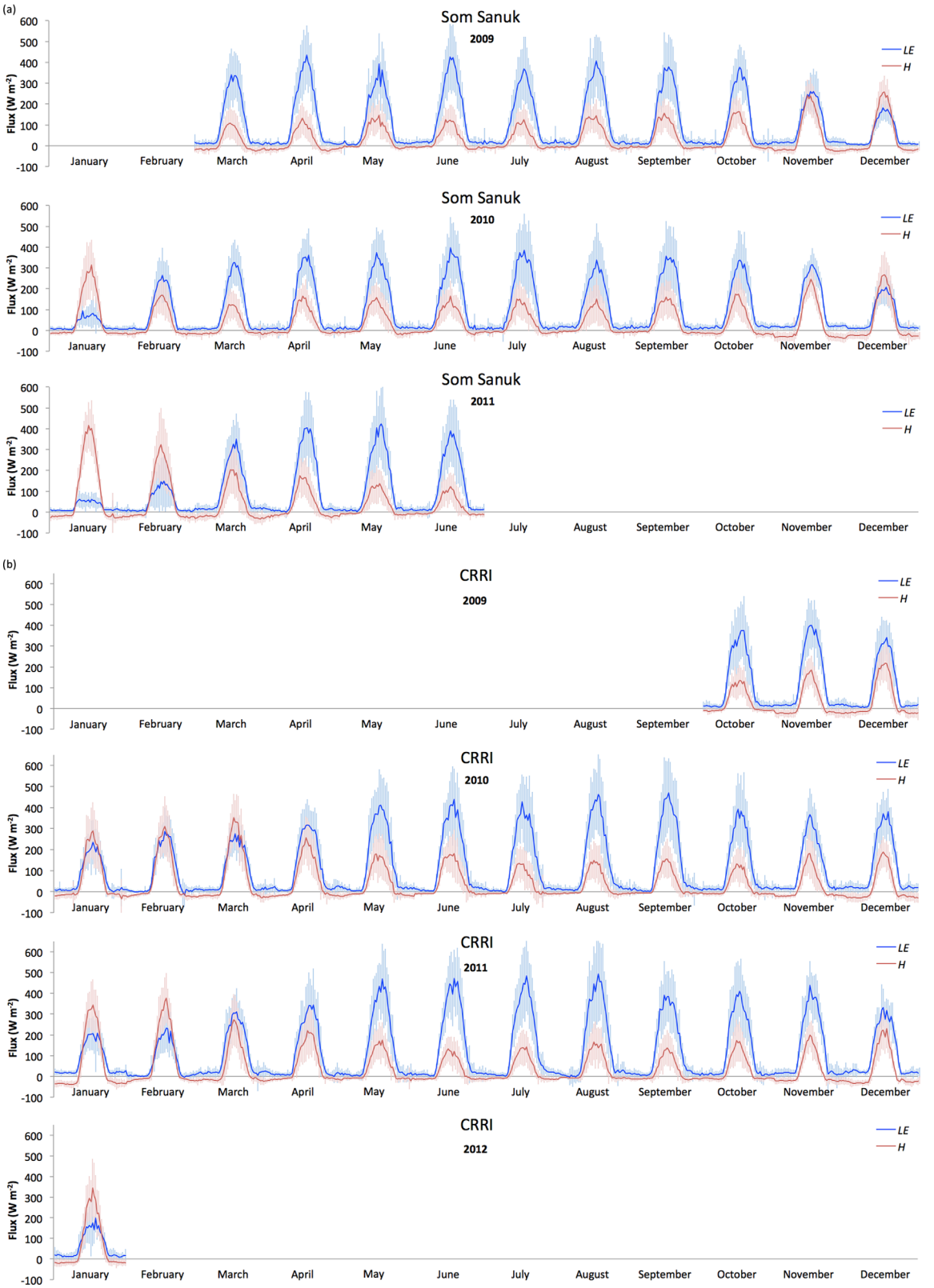

Figure 3. Monthly mean diurnal cycles of latent (blue) and sensible energy (red) flux (*LE* and *H*) at (a) Som Sanuk; and (b) CRRI. Shown are means (dark lines) ±1 standard deviation (vertical bars).

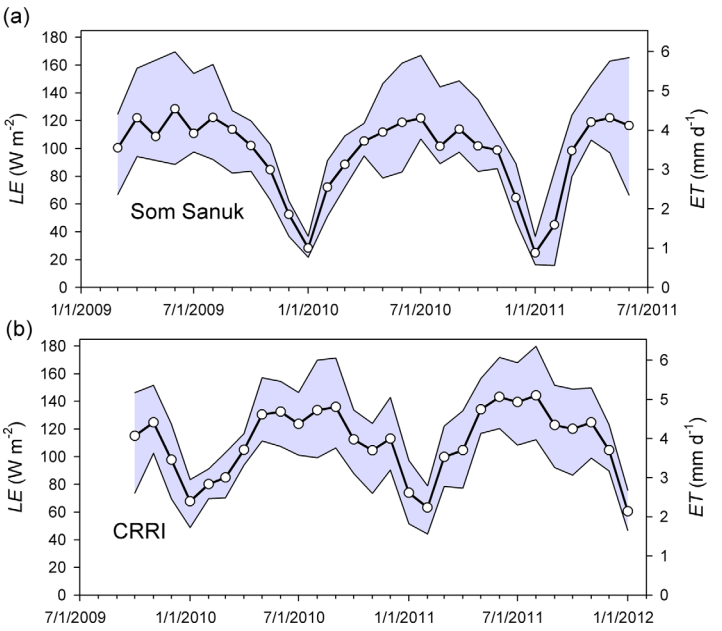

Figure 4. Mean monthly energy-closure-adjusted *LE* (left axis) and *ET* (right axis) at (a) Som Sanuk and (b) CRRI. The shaded area shows the range between the 15.9th and 84.1th percentiles of daily *LE* (*ET*).

Multiple linear regression using the five independent variables with the highest bivariate r^2 values results in these models for Som Sanuk ($LE_{Som\ Sanuk}$, N=375, $p \ll 0.0001$) and CRRI (LE_{CRRI}, N = 315, $p \ll 0.0001$):

$$LE_{Som\ Sanuk} = -123.6 + 0.523A + 24.1PAI + 1.08T + 0.028SM + 7.25VPD,\ r^2 = 0.881 \quad (11)$$

$$LE_{CRRI} = -34.2 + 0.668A + 13.0PAI - 1.70T + 0.042SM - 5.99VPD,\ r^2 = 0.691 \quad (12)$$

Coefficients of partial determination (pr^2) reveal that most of the explanation in equations (11) and (12) comes from *A* and *PAI*. The other predictors, *T*, *SM*, and *VPD* add 0–2% explained variance each. Clearly, multicollinearity accounts for the apparent stronger relationships with these variables seen in the bivariate results. For example, *T* at Som Sanuk and *SM* at CRRI have relatively high r^2 values in the bivariate results, likely the result of each being strongly correlated with *PAI*. More parsimonious models can be used with only slight reductions in explained variance:

$$LE_{Som\ Sanuk} = -85.9 + 0.560A + 27.1PAI,\ r^2 = 0.868 \quad (13)$$

$$LE_{CRRI} = -41.4 + 0.629A + 16.4PAI,\ r^2 = 0.650 \quad (14)$$

3.7. Variations in Midday Rain-Free Evapotranspiration in Relation to Potential Evapotranspiration

Potential *ET* incorporates all the atmospheric drivers of *ET*, allowing us to evaluate the response of the rubber plantation ecosystem to variations in evaporative demand. The annual cycles of midday rain-free LE_{pot_energy}, and $LE_{pot\_aerodynamic}$ are largely out of phase with each other at both sites (Figure 5); the energy term is high from the late dry season (beginning March, April, or May) to the end of the wet season (ending September, October, or November), while the aerodynamic term is highest during the dry season (from November or December to March). The annual cycle of $LE_{pot\_aerodynamic}$ has much greater amplitude than that of LE_{pot_energy}. Hence, LE_{pot} tends to be higher at both sites during the dry season.

The time series of the midday rain-free LE/LE_{pot} ratio is a measure of the responsiveness of each ecosystem to variations in evaporative demand because of month-to-month differences in available energy, vapor pressure deficit, and wind speed (Figure 6). Ecosystem response is expected to increase with increasing moisture availability, leaf area, and stomatal conductance. Note that the annual cycle of LE/LE_{pot} very closely follows the annual cycle of *PAI* at both sites. *PAI* explains 88 and 73% of the variance in LE/LE_{pot} at Som Sanuk and CRRI, respectively (Figure 7a). For comparison, mean monthly soil moisture explains only 24 and 48% of the variance in LE/LE_{pot} at the two sites (Figure 7b).

3.8. Variations in Midday Surface Conductance

The annual cycle of midday G_s (Figure 8) is similar for the two sites, with a steady increase from the minimum, near the time of leaf drop, to a maximum in the middle of the wet season, followed by a steady decline. The timing of this cycle is in phase with LE_{pot_energy}, and out of phase with $LE_{pot\_aerodynamic}$. Thus G_s is positively correlated with LE_{pot_energy} (r = 0.51 at Som Sanuk and 0.41 at CRRI) and negatively correlated with $LE_{pot\_aerodynamic}$ (r = −0.59 at Som Sanuk and −0.82 at CRRI).

Table 2. Results of Statistical Analysis of Latent Energy Flux Versus Biophysical Predictor Variables at a Daily Time Interval[a]

Som Sanuk	Bivariate: $LE = a + b*x$, N = 375				Correlation (r) Between Predictor Variables					Multiple Regression See Equation (11)
X	r^2	a	b	p-value		*A*	*PAI*	*T*	*SM*	Partial r^2
A	0.577	−44.2	1.014	≪0.0001	*A*					0.445
PAI	0.742	−48.4	36.560	≪0.0001	*PAI*	0.534				0.536
T	0.487	−138.1	8.790	≪0.0001	*T*	0.452	0.686			0.018
SM	0.098	5.7	0.138	≪0.0001	*SM*	0.378	0.233	0.072		0.019
VPD	0.038	63.8	18.380	0.0001	*VPD*	0.038	0.155	0.536	−0.471	0.021
CRRI	**Bivariate: $LE = a + b*x$, N = 315**				**Correlation (r) Between Predictor Variables**					**Multiple Regression See Equation (12)**
X	r^2	a	b	p-value		*A*	*PAI*	*T*	*SM*	Partial r^2
A	0.507	−32.9	0.916	≪0.0001	*A*					0.356
PAI	0.473	24.2	25.614	≪0.0001	*PAI*	0.507				0.160
T	0.035	−2.7	3.907	0.0008	*T*	0.403	0.309			0.012
SM	0.295	−99.7	0.166	≪0.0001	*SM*	0.302	0.528	−0.221		0.022
VPD	0.153	153.8	−37.799	≪0.0001	*VPD*	−0.105	−0.428	0.299	−0.731	0.005

[a]Note: *LE* = latent energy flux; *A* = available energy; *PAI* = plant area index; *T* = air temperature; *SM* = soil moisture; *VPD* = vapor pressure deficit; a = y-intercept; b = slope; p-value = significance statistic; wind speed did not have significant skill in predicting *LE* (not shown).

4. Discussion

4.1. Objective 1: Mean Annual Evapotranspiration of Rubber Plantations in Comparison with Other Tree-Dominated Land Covers

The results obtained here, particularly after energy closure adjustment, indicate that rubber does indeed maintain high annual *ET* rates, especially at the CRRI site where *ET*, at 1,459 mm yr^{-1}, approaches the highest values worldwide for land areas not affected by irrigation or lateral water flows (e.g., *Shi et al.* [2013], based on modeled *ET*; and *Jung et al.* [2011], based on observations). This is a remarkable result given the long dry season at both sites, where most land covers experience *ET* reduction due to drought stress during the dry season. This result is consistent with those of *Tan et al.* [2011], who found that *ET* of rubber in Xishuangbanna was exceptionally high, but contrasts with transpiration estimates in relatively dry areas of Northeastern Thailand [*Isarangkool Na Ayutthaya*, 2011].

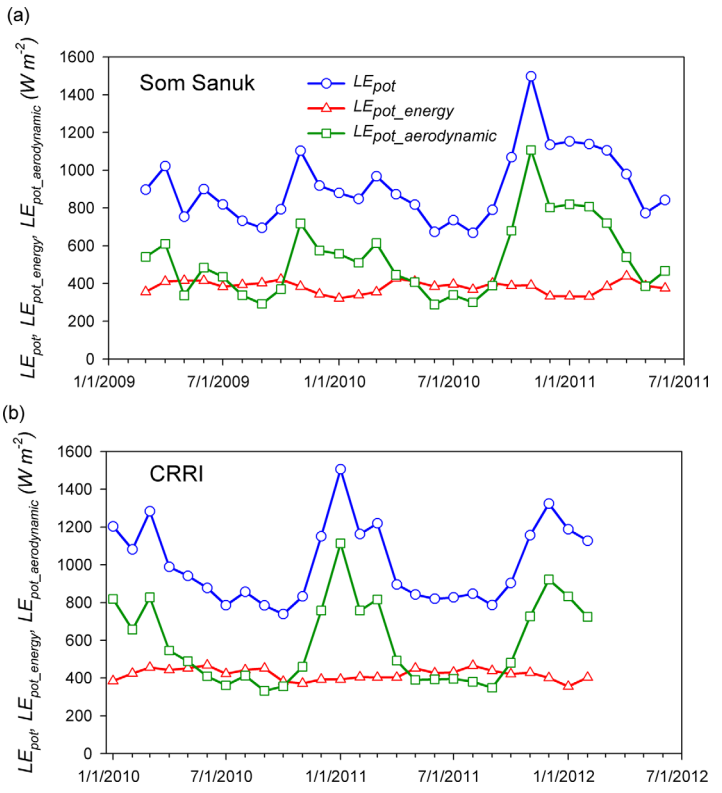

Figure 5. Mean monthly potential latent energy flux for midday rain-free periods (LE_{pot}; blue line with circles) and its components, the energy term (LE_{pot_energy}; red line with triangles) and the aerodynamic term ($LE_{pot\_aerodynamic}$; green line with squares) for rubber plantation sites at (a) Som Sanuk and (b) CRRI.

Comparing *ET* from our study sites and that of *Tan et al.* [2011] with values estimated for those locations by *Mueller et al.* [2013] suggests that *ET* for the dominant land covers near each study site is lower than that of rubber *ET* (Figure 9). For each of

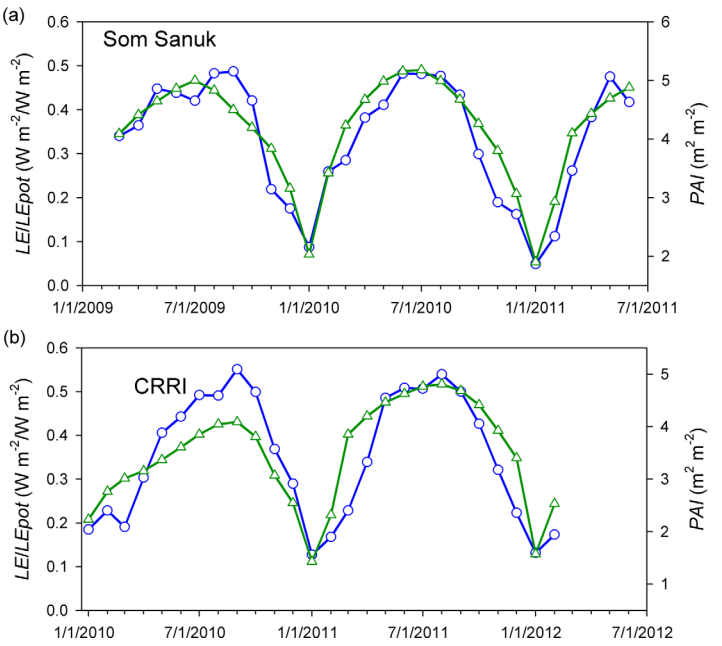

Figure 6. Mean monthly ratio of latent energy flux to potential latent energy flux for midday rain-free periods (LE/LE_{pot}; blue lines with circles) and mean monthly plant area index (*PAI*; green lines with triangles) for rubber plantation sites at (a) Som Sanuk and (b) CRRI.

the three sites, measured rubber *ET* exceeds the mapped *ET* estimates. For all three study sites, the adjusted rubber *ET* values were significantly greater ($p = 0.01$) than the mapped *ET* estimates (Xishuangbanna: 1125 versus 940 mm, +20%; Som Sanuk: 1211 versus 1043 mm, +16%; and CRRI: 1459 versus 1196 mm, +22%).

To further test whether rubber *ET* is indeed high relative to that of other land covers, we compiled measured and modeled *ET* rates for nonrubber land covers in the region or in similar climate regimes (Table 3). Mean annual rubber *ET* (1265 mm; n = 3 sites) is nearly as high as mean annual tropical rainforest *ET* (1311 mm; n = 6 sites), while mean annual *ET* of tropical seasonal forest (995 mm; n = 5 sites), and savanna (803 mm; n = 7 sites) are much lower. This pattern is more striking when comparing LE/R_n, the fraction of energy used for *ET* (last column of Table 3). Note that, despite the long dry season at rubber plantation sites, the mean value for rubber (0.725) is essentially equal to that of tropical rainforest (0.729) and much higher than that of tropical seasonal forest (0.594) and savanna (0.548).

Site by site comparisons also suggest that rubber has relatively high *ET* compared with other tree-covered sites with similar climate. *Tan et al.* [2011] report that annual rubber *ET* exceeds natural forest *ET* in Xishuangbanna by 21% (1125 versus 927 mm). Rubber *ET* at our Som Sanuk site in NE Thailand is much higher than

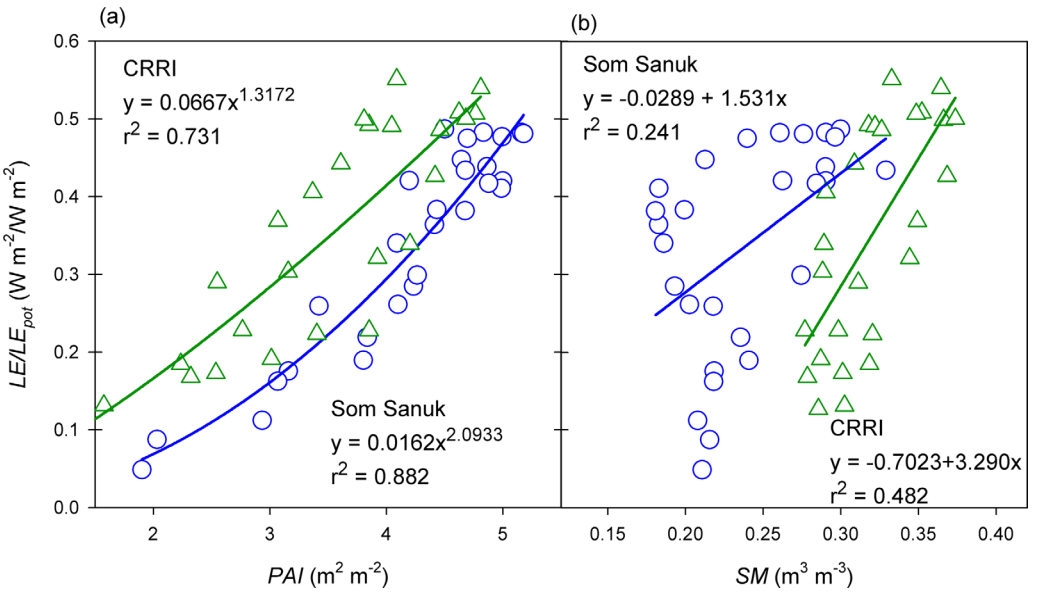

Figure 7. Mean monthly ratio of latent energy flux to potential latent energy flux for midday rain-free periods (LE/LE_{pot}) versus (a) mean monthly plant area index (*PAI*) and (b) mean monthly volumetric soil moisture content (*SM*) for rubber plantation sites at Som Sanuk (blue circles and blue lines) and CRRI (green triangles and green lines).

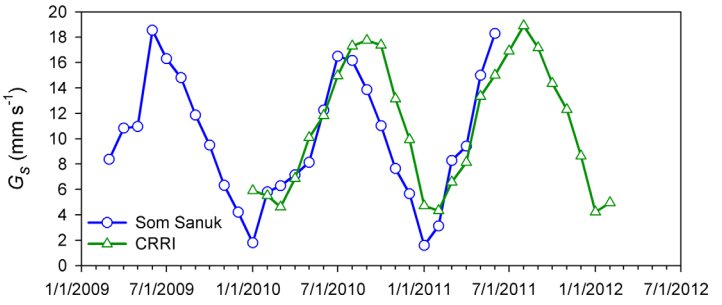

Figure 8. Mean monthly surface conductance for midday rain-free periods (G_s) for Som Sanuk (blue line with circles) and CRRI (green line with triangles) rubber plantation sites.

that of tropical seasonal forest (Kog Ma, northern Thailand) [*Tanaka et al.*, 2003] and teak plantation (Mae Moh, northern Thailand) *Igarashi et al.*, 2015a, 2015b] in northern Thailand, but this comparison is confounded by the higher mean annual precipitation at the Som Sanuk site (Table 3). Perhaps a better reference site for Som Sanuk is the seasonal transitional forest in Sinop, Mato Grosso, Brazil, which has similar mean precipitation and net radiation, although a less seasonal moisture regime than for NE Thailand. Compared with forest *ET* at Sinop [*Costa et al.*, 2010], rubber *ET* at Som Sanuk is higher by 8% (1211 mm versus 1118 mm; Table 3). For our Cambodia site, rubber *ET* is higher than evergreen forest *ET* at Kampong Thom [*Nobuhiro et al.*, 2007] by 28% (1459 versus 1140 mm) or by 36% when normalized by R_n (Table 3).

4.2. Objective 2: Roles of Phenological and Environmental Controls on the Annual Cycle of Evapotranspiration in Rubber Plantations

To help identify the mechanisms that lead to high annual *ET* by rubber, we examine the *ET* annual cycle (Figures 3 and 4) in relation to biological (Figures 2 and 8) and environmental cycles (Figures 1 and 5). High annual *ET* by rubber is partly the result of high late dry season water use, a remarkable feature of the *ET* time series at both sites related to rubber's brevideciduous phenology. Both *PAI* and *ET* rapidly increase from their annual lows during January to near wet season values before the start of the rainy season (Figures 2 and 4). By April, *ET* is equal to mean May–September *ET* at Som Sanuk and reaches about 78% of the May–September rate at CRRI. This high late dry season *ET* in rubber is facilitated by rapid refoliation following leaf drop in January despite soil moisture levels near their lowest point at that time (Figure 1). This implies that rubber trees are able to access deep soil water reserves. In Xishuangbanna, *Guardiola-Claramonte et al.* [2008] showed that deep layer water extraction under rubber increased as the surface soil dried. *Gonkhamdee et al.* [2009] found that fine root growth in the deep soil layer (below the 300 cm depth) at the Baan Sila rubber plantation became active only in the dry season. We observed that, as surface soil moisture declined during each dry season, the rate of extraction of soil water declined much less from layers below about 1.2 m at Som Sanuk and below about 1.7 m at CRRI compared with extraction from shallow layers (see supporting information Figure S3). By the end of the dry season, more than half of the water being extracted from soil was derived from those deep soil layers at each site. At our CRRI study site, as soon as

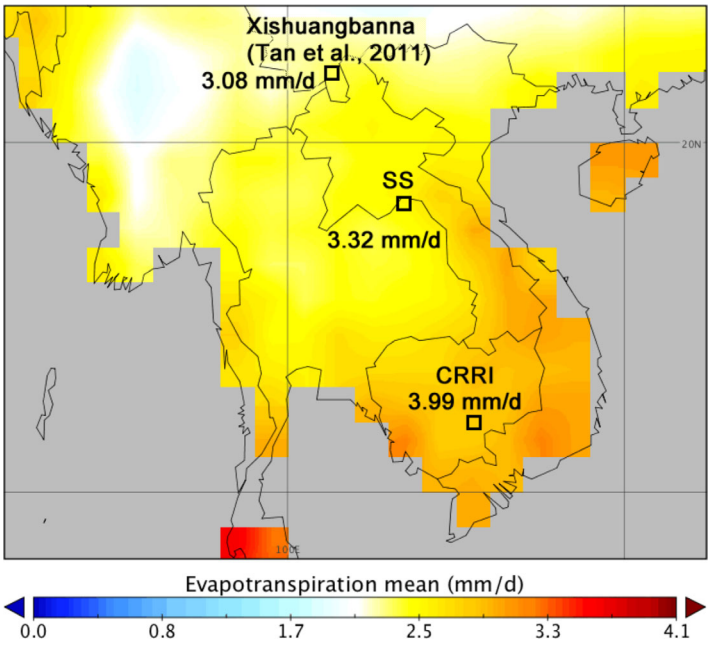

Figure 9. Mean annual energy-closure-adjusted evapotranspiration (*ET*) at tower sites from this study and a site in Xishuangbanna reported by *Tan et al.* [2011] shown against a map of estimated regional *ET* from the LandFlux-EVAL merged benchmark synthesis products of ETH Zurich produced under the aegis of the GEWEX and ILEAPS projects [*Mueller et al.*, 2013].

Table 3. Summary of Evapotranspiration (*ET*) Estimates for Tropical Tree-Dominated Ecosystems

Location	Mean Annual *P* (mm)	Mean Annual R_{net} (W m^{-2})	Mean Annual *ET* (mm)	Mean *LE* (W m^{-2})	*LE/Rnet* ((W m^{-2}) (W m^{-2})$^{-1}$)
Tropical rainforest					
Pasoh, Malaysia[a]	1865	144.2	1287[b]	99.3[b]	0.689
Lambir Hills, Borneo[c]	2600	134.3	1323[b]	102.7[b]	0.765
Manaus, Amazonas, Brazil[d]	3068	135.0	1362[e]	105.8[e]	0.783
Santarém, Pará, Brazil[d]	2082	128.8	1362[e]	105.8[e]	0.821
Jaru, Rondonia, Brazil[d]	1644	135.8	1300[e]	100.9[e]	0.743
Volcano, Hawai'i[f]	2401	166.5	1232[b]	95.7[b]	0.575
Mean Tropical Rainforest	2277	140.8	1311	101.7	0.729
Tropical seasonal forest					
Xishuangbanna, China[g]	1534	119.2	927[b]	72.0[b]	0.604
Chiang Mai, Thailand[h]	1573	115.7	812[i]	63.0[i]	0.545
Kampong Thom, Cambodia[j]	1600	161.3	1140[k]	88.5[k]	0.549
Mae Moh, Northern Thailand[l]	1335	125.3	977[m]	75.9[m]	0.619
Sinop, Mato Grosso, Brazil[d]	1826	130.2	1118[e]	86.8[e]	0.667
Mean Tropical Seasonal Forest	1574	130.3	995	77.6	0.597
Savanna					
Brasilia, Brazil[n]	1440	135.0	1060[b]	82.3[b]	0.610
Australia[o]	1756		958[p]	74.4[p]	
Sunsunes, Venezuela[q]	1066		732[r]	56.8[r]	
Aguasay, Venezuela[q]	1000		771[r]	59.9[r]	
Brasilia, Brazil[n]	1440	134.0	840[b]	65.2[b]	0.487
Aguasay, Venezuela[q]	1000		538[r]	41.8[r]	
Santa Barbara, Venezuela[q]	1100		721[r]	56.0[r]	
Mean Savanna	1257	134.5	803	62.3	0.548
Rubber plantation					
Xiushuangbanna, China[g]	1504	123.3	1125[b]	87.4[b]	0.709
Som Sanuk, Thailand[s]	2145	129.5	1211[b]	93.5[b]	0.722
CRRI, Cambodia[s]	1439	151.0	1459[b]	112.5[b]	0.745
Mean Rubber Plantation	1696	134.6	1265	97.8	0.725

[a] *Kosugi et al.* [2012].
[b] Eddy covariance results adjusted to achieve energy closure.
[c] *Kumagai et al.* [2005] and *Kume et al.* [2011].
[d] *Costa et al.* [2010].
[e] Eddy covariance results filtered for energy closure.
[f] *Giambelluca et al.* [2009a].
[g] *Tan et al.* [2011].
[h] *Tanaka et al.* [2003].
[i] *ET* derived from catchment water balance observations.
[j] *Nobuhiro et al.* [2007].
[k] *ET* derived from Bowen ratio observations.
[l] *Igarashi et al.* [2015b].
[m] Based on eddy covariance observations—no energy closure adjustment (energy closure ratio: 0.72).
[n] *Giambelluca et al.* [2009b].
[o] *Hutley et al.* [2000].
[p] Eddy covariance results had energy closure error of 8 to 15%—no adjustment was made.
[q] *San José et al.* [2008].
[r] Eddy covariance estimates had acceptable energy closure without adjustment.
[s] This study.

rains began, deep layer water extraction ceased (Figure 1b). Thus, rubber tree roots are able to respond to the changing soil moisture distribution, continue to access soil water from deep in the profile when the upper soil layers are dry, and thus maintain high *ET* rates late in the dry season.

In other studies, high late dry season *ET* at natural forest and tree plantation sites in the region has been restricted to sites at which soil moisture availability at relatively shallow depths is augmented by lateral water flows. For example, at Kampong Thom, Cambodia, the shallow water table plays a role in supplying water during the dry season [*Nobuhiro et al.*, 2007]. More representative sites, such as dry evergreen forest at Sakaerat, Thailand [*Pinker et al.*, 1980], disturbed dry dipterocarp forest at Tak, Thailand [*Toda et al.*, 2002], and teak plantation at Mae Moh, Thailand [*Igarashi et al.*, 2015a, 2015b], experience their annual minimum *ET* late in the dry season, because of low soil water availability and reductions in leaf area.

G_s in rubber begins increasing immediately following leaf flushing at both sites (Figure 8), but by the end of the dry season is still less than half the peak wet-season values despite high *PAI* (Figure 2). Reduced conductance affects the partitioning of energy, as seen clearly in the relatively high values of *H* during March and April at CRRI (Figure 3b). Thus, rubber trees are controlling water use by restricting stomatal conductance to some extent in the late dry season [*Kumagai et al*., 2015]. However, despite stomatal control, *ET* rates are high because of the high evaporative demand conditions prevailing in the dry season—at Som Sanuk, midday LE_{pot} reaches its annual maximum in April; at CRRI, mean March–April midday LE_{pot} is only 4% lower than the May–September mean (Figure 5).

During the wet season, daily rubber *ET* reaches very high rates (up to 6 mm d^{-1}) at both sites. *Tan et al*. [2011, supporting information, Figure S3] showed that *ET* of rubber was similar to that of forest in Xishuangbanna in the late dry season, but exceeded forest *ET* by around 0.7–1.1 mm d^{-1} during June–December. For forests and tree plantations in the region, wet season *ET* tends to be higher, in general, for sites dominated by deciduous trees. For example, while evergreen forest at Kog Ma, Thailand [*Tanaka et al*., 2008] and Kampong Thom, Cambodia [*Nobuhiro et al*., 2007] had wet season *ET* of about 2.0–3.0 and 2.0 mm d^{-1}, respectively, deciduous dipterocarp forest in Tak, Thailand [*Toda et al*., 2002] and teak plantation in Mae Moh, Thailand [*Igarashi et al*., 2015a, 2015b] had wet season *ET* of 4.5 (if adjusted for energy closure) and ~4.4 mm d^{-1}, respectively. *Baldocchi et al*. [2010] showed that, in mediterranean climates, deciduous oaks achieved annual *ET* totals similar to those of evergreen oaks, because of much higher gas exchange rates in deciduous trees during the wet season.

At our two study sites, large annual *ET* totals are generated despite a significant period of defoliation and despite very low rainfall for half the year. The chief mechanisms by which rubber achieves high annual *ET* totals are: (1) short leafless period and rapid attainment of high leaf area during the late dry season; unlike other deciduous trees in the region, such as teak [*Igarashi et al*., 2015a, Figure 2d], rubber refoliates quickly (Figure 2); (2) deep soil water extraction; *ET* of forests in the region is strongly moisture limited in the late dry season; rubber is able to utilize deep soil water reserves to maintain high transpiration late in the dry season (supporting information Figure S3; (3) high transpiration throughout the wet season (Figure 4); rubber, like other deciduous trees, compensates for a shortened growing season by maintaining high gas exchange rates during the wet season.

4.3. Objective 3: Environmental Controls and Spatial Differences in Evapotranspiration of Rubber in MSEA

The weak response of *ET* to *SM* variation at Som Sanuk and the muted response at CRRI (Table 2) contrast with the findings of *Isarangkool Na Ayutthaya* [2011], who found that daily transpiration in rubber trees at a plantation in Baan Sila, Buri Ram Province, NE Thailand, was strongly responsive to *SM* variations. Similarly, we found that *ET* was only weakly related to *VPD*, and had opposite effects at our two sites (Table 2). In a related paper, *Kumagai et al*. [2015] showed that stomatal conductance derived from the data at our study sites is negatively related to *VPD* at both sites, but is much more strongly related at CRRI than Som Sanuk. *Isarangkool Na Ayutthaya* [2011] found rubber transpiration to be positively related to *VPD*, indicating that the effects of *VPD* on evaporative demand outweighed effects on stomatal conductance, up to *VPD* = 1.6–1.8 kPa. Above that level, transpiration was not responsive to *VPD*. At another study site in northeastern Thailand, *Clermont-Dauphin et al*. [2013] found that rubber tree growth was limited mainly by high *VPD* in the dry season (and also soil waterlogging in the wet season) rather than by low soil moisture. The contrasting results on the response of rubber *ET* to atmospheric and soil drought mainly point to differences between rubber growing areas with adequate rainfall (represented by Xishuangbanna and our two study sites) and marginal (drier) rubber growing areas (represented by the Baan Sila site).

For our sites, we noted that midday rain-free G_s (Figure 8) is positively correlated with LE_{pot_energy} and negatively correlated with $LE_{pot\_aerodynamic}$ (Figure 5). This finding confirms that the biological controls exerted by rubber trees promote very high gas exchange—both transpiration and photosynthesis—during the wet season, when G_s (Figure 8) and radiative input (Figure 1) are both high, and limit excessive water loss, perhaps avoiding xylem cavitation, during the late dry season, when G_s is low (Figure 8) and *VPD* is high (Figure 1). The sustained late dry season *ET* contributes to the very high annual totals. But, because the strong biological control on *ET* associated with the brevideciduous leaf phenology acts counter to the annual cycle in

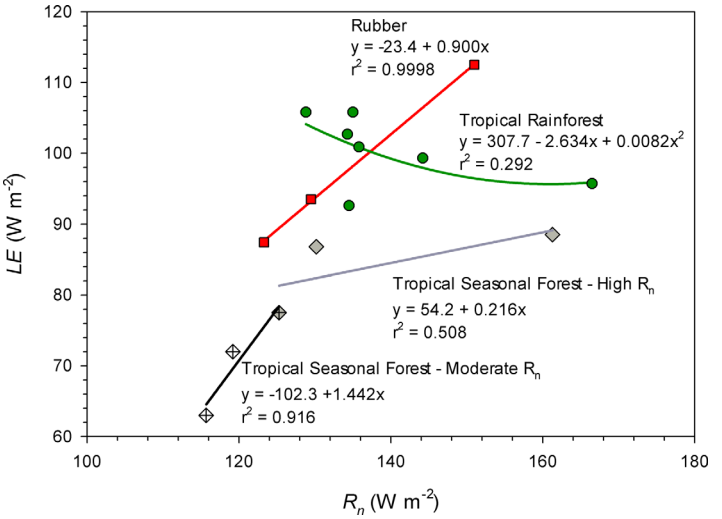

Figure 10. Mean annual latent energy flux (*LE*) as a function of mean annual net radiation (R_n) for tree-dominated tropical ecosystems, including tropical rainforest (dark green circles), seasonal tropical forest (sites with moderate R_n: diamonds with crosses; sites with high R_n: gray diamonds), and rubber plantations (red squares). Data are given in Table 3. Seasonal tropical forest sites are separated into moderate and high R_n environments (arbitrarily divided at $R_n \cong 125$ W m^{-2}), with Mae Moh site included in samples for both regressions.

aerodynamic moisture demand (Figure 5), potentially damaging water stress is apparently avoided at our field sites.

Analysis of rubber *LE* response to biophysical variables (Table 2) confirmed the strong influence of *A*. Spatial variations in *A* mainly reflect spatial patterns of R_n. *LE* as a proportion of R_n differs by land cover (Table 3), but how does *LE* of each land cover type respond to spatial differences in R_n? Plotting mean annual *LE* versus R_n for various tree-dominated tropical ecosystems (Figure 10) shows that *LE* of native seasonal tropical forest ecosystems increases relatively slowly with increasing R_n for sites with mean R_n above ~125 W m^{-2}. Tropical rainforest *ET* appears to decrease slightly with higher R_n. As expected, for areas with higher R_n, which implies ecologically drier conditions, these ecosystems exert significant stomatal control such that *ET* does not continue to increase with increasing energy availability. In contrast, rubber plantations exhibit a strong positive response (spatially) to increasing R_n across the three sites with available data. The apparently risky gas exchange strategy of rubber, i.e., freely increasing gas exchange rates across the available energy gradient, might be the result of having evolved in the wet rainforests of the equatorial Amazon basin, where the risk of catastrophic water stress damage is low. The fast growth rates that make this species attractive as a commercial crop are likely to be explained, in part, by physiological traits evolved in a constantly wet environment [c.f., *Tan et al.*, 2011].

The results of *Isarangkool Na Ayutthaya et al.* [2011] demonstrate that the relationship between *ET* and R_n shown in Figure 10 pertains only to sites with sufficient available water. For the Baan Sila study, annual rainfall was relatively low (<1200 mm), several dry periods of 10–20 days were experienced throughout the rainy season, and maximum leaf area index was only 3.9 m^2 m^{-2} [*Isarangkool Na Ayutthaya et al.*, 2011]. Under those restricted moisture conditions, rubber transpiration was more responsive to soil moisture variability and *ET* did not attain exceptionally high annual totals. Similarly, rubber tree growth [*Rantala*, 2006] and latex yield [*Raj et al.*, 2005] are known to be strongly limited by moisture availability in areas subject to growing season drought.

With stand level *ET* estimates available for only three rubber plantation sites in the region (Figure 9) our ability to map spatial patterns of rubber *ET* is limited. Nevertheless, the relationships with environmental variables suggest that *ET* is high relative to other land covers (Figure 10) and is mainly limited by available energy in areas where rubber is commercially successful (and where cultivation is likely to expand in the future). The extension of rubber cultivation into nontraditional growing areas has included planting in some areas with marginal environmental conditions, such as relatively dry areas of northeastern Thailand. However, it is reasonable to expect rubber expansion to be focused mainly in areas with more favorable conditions, i.e., areas where conditions promote both viable latex yields and high *ET*.

5. Conclusions

Our results, along with those of *Tan et al.* [2011] demonstrate that rubber plantations support high *ET* rates. The results of eddy covariance measurements in two Southeast Asian rubber plantations show that mean annual *ET* is high in comparison with regional *ET* estimates and *ET* measured or modeled for nonrubber

land cover types in the region or other areas with a similar climate. The high annual *ET* of rubber results from high late dry season rates, facilitated by rapid refoliation after leaf drop and by access to deep soil water, and from high wet season rates, a characteristic of deciduous trees. *ET* in rubber plantations is strongly controlled by variations in available energy and leaf area, and is only weakly related to soil moisture and vapor pressure deficit. Rubber trees at the study sites vary leaf area and stomatal conductance such that bulk surface conductance is positively correlated with the annual cycle in energy-driven evaporative demand (enabling high wet season gas exchange rates) and negatively correlated with the atmospheric-dryness-driven demand (preventing injury due to water stress). Spatial differences in rubber *ET* across three sites in MSEA with available stand level data are explained by linear increases with increasing energy availability, in contrast to tropical rainforest and tropical seasonal forest, for which *ET* levels off toward sites with higher energy availability.

As the area devoted to cultivation of rubber and other tree planation species in the region expands, the relatively high *ET* rates of rubber should motivate resource managers to be vigilant for possible effects on water flows. In a region highly dependent on paddy rice cultivation, it is possible that widespread rubber cultivation could cause greater depletion of basin water storage at the end of the dry season (because of greater dry season *ET*), delaying the onset of wet-season streamflow needed for irrigation, and thereby shortening the rice growing season [c.f., *Guardiola-Claramonte et al*., 2010]. Because alien tree species selected for use in commercial plantations are generally fast growing, it is reasonable to ask whether some of the other plantation species also share the trait of high water use with rubber. In that case, the rapid shift toward various types of tree plantations as the emerging dominant land cover of the region [*Li and Fox*, 2011; *Fox*, 2012] could have impacts on water and food security in the region. These concerns should be balanced against the economic and social benefits of rubber cultivation, which provides for the livelihoods of millions of smallholders and their employees.

Acknowledgments
This study was conducted as a cooperative project between Cambodian Rubber Plantation Department, Cambodian Rubber Research Institute (CRRI), the University of Hawai'i (USA), and Kyushu University (Japan), and through a memorandum of understanding between the University of Hawai'i and Kasetsart University (Thailand), with support from NASA grants NNG04GH59G and NNX08AL90G, the Global COE (Centers of Excellence) Program (GCOE) of the Japan Society for the Promotion of Science (JSPS), a grant from the Ministry of Agriculture, Forestry and Fisheries, Japan for the project "Estimation and simulation of carbon stock change of tropical forest in Asia (2011–2014)," a Grant-in-Aid for Scientific Research (23405028), a grant from the Ministry of Education, Science and Culture, Japan for the project "Program for risk information on climate change," and a grant from Kyushu University. A.D.Z. was supported by National University of Singapore (NUS) grant R-109-000-092-133 and Asia-Pacific Network for Global Change Research (APN) grant ARCP2008-01CMY. M.H. was supported by the U.S. Department of Energy (DOE) Biological and Environmental Research (BER) through the Terrestrial Ecosystem Science program. The Pacific Northwest National Laboratory (PNNL) is operated for the U.S. DOE by Battelle Memorial Institute under contract DE-AC05-76RL01830. We are grateful for the assistance provided by the staff of CRRI and other contributors, including Tsuyoshi Kajisa, Khun Kakada, Nobuya Mizoue, Makiko Tateishi, and Tetsukazu Yahara. Data related to this publication are archived at https://sites.google.com/a/hawaii.edu/ecohydrology_lab/home. This study made use of the LandFlux-EVAL merged benchmark synthesis products of ETH Zurich produced under the aegis of the GEWEX and ILEAPS projects (http://www.iac.ethz.ch/url/research/LandFlux-EVAL/).

References

Baldocchi, D. D., B. B. Hicks, and T. P. Meyers (1988), Measuring biosphere-atmosphere exchanges of biologically related gases with micrometeorological methods, *Ecology*, *69*, 1331–1340.

Baldocchi, D. D., S. Ma, S. Rambal, L. Misson, J.-M. Ourcival, J.-M. Limousin, J. Pereira, and D. Papale (2010), On the differential advantages of evergreenness and deciduousness in mediterranean oak wooklands: A flux perspective, *Ecol. Appl.*, *20*, 1583–1597.

Beck, H. E., L. A. Bruijnzeel, A. I. J. M. Van Dijk, T. R. McVicar, F. N. Scatena, and J. Schellekens (2013), The impact of forest regeneration on streamflow in 12 mesoscale humid tropical catchments, *Hydrol. Earth Syst. Sci.*, *17*(7), 2613–2635.

Bosch, J. M., and J. D. Hewlett (1982), A review of catchment experiments to determine the effect of vegetation changes on water yield and evapotranspiration, *J. Hydrol.*, *55*, 3–23.

Brown, A. E., A. W. Western, T. A. McMahon, and L. Zhang (2013), Impact of forest cover changes on annual streamflow and flow duration curves, *J. Hydrol.*, *483*, 39–50, doi:10.1016/j.jhydrol.2012.12.031.

Bruijnzeel, L. A. (2004), Hydrological functions of tropical forests: Not seeing the soil for the trees, *Agric. Ecosyst. Environ.*, *104*, 185–228.

Clermont-Dauphin, C., N. Suvannang, C. Hammecker, V. Cheylan, P. Pongwichian, and F. C. Do (2013), Unexpected absence of control of rubber tree growth by soil water shortage in dry subhumid climate, *Agron. Sustain. Dev.*, *33*, 531–538, doi:10.1007/s13593-012-0129-2.

Costa, M. H., M. C. Biajoli, L. Sanches, A. C. M. Malhado, L. R. Hutyra, H. R. da Rocha, R. G. Aguiar, and A. C. de Araújo (2010), Atmospheric versus vegetation controls of Amazonian tropical rain forest evapotranspiration: Are the wet and seasonally dry rain forests any different? *J. Geophys. Res.*, *115*, G04021, doi:10.1029/2009JG001179.

Falge, E., et al. (2001), Gap filling strategies for defensible annual sums of net ecosystem exchange, *Agric. For. Meteorol.*, *107*, 43–69, doi:10.1016/S0168-1923(00)00225-2.

Fisher, J. B., et al. (2009), The land–atmosphere water flux in the tropics, *Global Change Biol.*, *15*, 2694–2714.

Fox, J. (2012), The production of forests, Tree cover transitions in Northern Thailand, Northern Laos, and Southern China, in *The Social Life of Forests*, edited by S. Hecht, K. Morrison, and C. Padoch, Univ. of Chicago Press, Chicago.

Fox, J., and J.-C. Castella (2013), Expansion of rubber (*Hevea brasiliensis*) in mainland Southeast Asia: What are the prospects for small holders?, *J. Peasant Stud.*, *40*, 155–170.

Fox, J., J. Krummel, S. Yarnasarn, M. Ekasingh, and N. Podger (1995), Land-use and landscape dynamics in Northern Thailand: Assessing change in three upland watersheds since 1954, *Ambio*, *24*, 328–334.

Fox, J., J.-C. Castella, and A. D. Ziegler (2014), Swidden, rubber and carbon: Can REDD+ work for people and the environment in Montane Mainland Southeast Asia? *Global Environ. Change*, *40*, 318–326, doi:10.1016/j.gloenvcha.2013.05.011.

Franssen, H. J. H., R. Stöckli, I. Lehner, E. Rotenberg, and S. I. Seneviratne (2010), Energy balance closure of eddy-covariance data: A multisite analysis for European FLUXNET stations, *Agric. For. Meteorol.*, *150*, 1553–1567.

Giambelluca, T. W., R. E. Martin, G. P. Asner, M. Huang, R. G. Mudd, M. A. Nullet, J. K. DeLay, and D. Foote (2009a), Evapotranspiration and energy balance of native wet montane cloud forest in Hawai'I, *Agric. For. Meteorol.*, *149*, 230–243, doi:10.1016/j.agrformet.2008.08.004.

Giambelluca, T. W., F. G. Scholz, S. J. Bucci, F. C. Meinzer, G. Goldstein, W. A. Hoffmann, A. C. Franco, and M. P. Buchert (2009b), Evapotranspiration and energy balance of Brazilian savannas with contrasting tree density, *Agric. For. Meteorol.*, *149*, 1365–1376, doi:10.1016/j.agrformet.2009.03.006.

Gonkhamdee, S., J.-L. Maeght, F. C. Do, and A. Pierret (2009), Growth dynamics of fine *Hevea brasiliensis* roots along a 4.5-m soil profile, *Khon Kaen Agric. J.*, *37*, 265–276.

Guardiola-Claramonte, M., P. Troch, A. D. Ziegler, T. W. Giambelluca, J. B. Vogler, and M. A. Nullet (2008), Local hydrological effects of introducing non-native vegetation in a tropical catchment, *Ecohydrology*, *1*, 13–22, doi:10.1002/eco.3.

Guardiola-Claramonte, M., P. Troch, A. Ziegler, T. Giambelluca, J. Vogler, and M. Nullet (2010), Hydrologic effects of the expansion of rubber (*Hevea brasiliensis*) in a tropical catchment, *Ecohydrology*, *3*, 306–314, doi:10.1002/eco.110.
Hibbert, A. R. (1965), Forest treatment effects on water yield, in *International Symposium on Forest Hydrology, Proceedings of a National Science Foundation Advanced Science Seminar*, edited by W. E. Sopper and H. W. Lull, pp. 527–543, Pergamon Press, London, U. K.
Hoover, M. D. (1944), Effect of removal of forest vegetation upon water yields, *Trans. AGU*, *6*, 969–75.
Hu, H., W. Liu, and M. Cao (2008), Impact of land use and land cover changes on ecosystem services in Menglun, Xishuangbanna, southwest China, *Environ. Monit. Assess.*, *146*, 147–156.
Hutley, L. B., A. P. O'Grady, and D. Eamus (2000), Evapotranspiration from Eucalyptus open-forest savanna of Northern Australia, *Funct. Ecol.*, *14*, 183–194.
Igarashi, Y., T. Kumagai, N. Yoshifuji, T. Sato, N. Tanaka, K. Tanaka, M. Suzuki, and C. Tantasirin (2015a), Environmental control of canopy stomatal conductance in a tropical deciduous forest in northern Thailand, *Agric. For. Meteorol.*, *202*, 1–10, doi:10.1016/j.agrformet.2014.11.013.
Igarashi, Y., G. G. Katul, T. Kumagai, N. Yoshifuji, T. Sato, N. Tanaka, H. Fujinami, M. Suzuki, and C. Tantasirin (2015b), Separating physical and biological controls on long-term evapotranspiration fluctuations in a tropical deciduous forest subjected to monsoonal rainfall, *J. Geophys. Res. Biogeosci.*, *120*, 1262–1278, doi:10.1002/2014JG002767.
Isarangkool Na Ayutthaya, S., F. C. Do, K. Pannangpetch, J. Junjittakarn, J.-L. Maeght, A. Rocheteau, and H. Cochard (2011), Water loss regulation in mature *Hevea brasiliensis*: Effects of intermittent drought in the rainy season and hydraulic regulation, *Tree Physiol.*, *31*, 751–762, doi:10.1093/treephys/tpr058.
Jung, M., et al. (2011), Global patterns of land-atmosphere fluxes of carbon dioxide, latent heat, and sensible heat derived from eddy covariance, satellite, and meteorological observations, *J. Geophys. Res.*, *116*, G00J07, doi:10.1029/2010JG001566.
Kobayashi, N., T. Kumagai, Y. Miyazawa, K. Matsumoto, M. Tateishi, T. K. Lim, R. G. Mudd, A. D. Ziegler, T. W. Giambelluca, and Y. Song (2014), Transpiration characteristics of a rubber plantation in central Cambodia, *Tree Physiol.*, *34*, 285–301, doi:10.1093/treephys/tpu009.
Kochendorfer J., T. P. Meyers, J. M. Frank W. J. Massman, and M. W. Heuer (2012), How well can we measure the vertical wind speed? Implications for fluxes of energy and mass, *Boundary Layer Meteorol.*, *145*, 383–398.
Kosugi, Y., S. Takanashi, M. Tani, S. Ohkubo, N. Matsuo, M. Itoh, S. Noguchi, and A. Rahim Nik (2012), Effect of inter-annual climate variability on evapotranspiration and canopy CO2 exchange of a tropical rainforest in Peninsular Malaysia, *J. Forest Res.*, *17*, 227–240, doi:10.1007/s10310-010-0235-4.
Kumagai, T., T. M. Saitoh, Y. Sato, H. Takahashi, O. J. Manfroi, T. Morooka, K. Kuraji, M. Suzuki, T. Yasunari, and H. Komatsu (2005), Annual water balance and seasonality of evapotranspiration in a Bornean tropical rainforest, *Agric. For. Meteorol.*, *128*, 81–92, doi:10.1016/j.agrformet.2004.08.006.
Kumagai, T., et al. (2015), How do rubber (*Hevea brasiliensis*) plantations cope with seasonal drought in northern Thailand and central Cambodia?, *Agric. For. Meteorol.*, *213*, 10–22, doi:10.1175/JCLI-D-15-0088.1.
Kume, T., N. Tanaka, K. Kuraji, H. Komatsu, N. Yoshifuji, T. M. Saitoh, M. Suzuki, and T. Kumagai (2011), Ten-year evapotranspiration estimates in a Bornean tropical rainforest, *Agric. For. Meteorol.*, *151*, 1183–1192, doi:10.1016/j.agrformet.2011.04.005.
Law, B. E., and R. H. Waring (1994), Remote sensing of leaf area index and radiation intercepted by understory vegetation, *Ecol. Appl.*, *4*, 272–279.
Leuning, R., E. van Gorsel, W. J. Massman, and P. R. Isaac (2012), Reflections on the surface energy imbalance problem, *Agric. For. Meteorol.*, *156*, 65–74.
Li, H., T. M. Aide, Y. Ma, W. Liu, and M. Cao (2007), Demand for rubber is causing the loss of high diversity rain forest in SW China, *Biodivers. Conserv.*, *16*, 1731–1745, doi:10.1007/s10531-006-9052-7.
Li, H., Y. Ma, T. M. Aide, and W. Liu (2008), Past, present and future land-use in Xishuangbanna, China and the implications for carbon dynamics, *For. Ecol. Manage.*, *255*, 16–24, doi:10.1016/j.foreco.2007.06.051.
Li, Z., and J. Fox (2011), Mapping rubber tree growth in mainland Southeast Asia using time-series MODIS 250 m NDVI and statistical data, *Appl. Geogr.*, *32*, 420–432.
Malmer, A., D. Murdiyarso, and U. Ilstedt (2010), Carbon sequestration in tropical forests and water: A critical look at the basis for commonly used generalizations, *Global Change Biol.*, *16*(2), 599–604.
Manivong, V., and R. A. Cramb (2008), Economics of smallholder rubber expansion in northern Laos, *Agroforest. Syst.*, *74*, 113–125.
Mann, C. C. (2009), Addicted to rubber, *Science*, *325*(5940), 564–566, doi:10.1126/science.325_564.
Meyfroidt, P., and E. F. Lambin (2011), Global forest transition: Prospects for an end to deforestation, *Annu. Rev. Environ. Resour.*, *36*, 343–371, doi:10.1146/annurev-environ-090710-143732.
Monsi, M., and T. Saeki (1953), Über den Lichtfaktor in den Pflanzengesellschaften und seine Bedeutung für die Stoffproduktion, *Jpn. J. Bot.*, *14*, 22–52.
Monsi, M., and T. Saeki (2005), On the factor light in plant communities and its importance for matter production, *Ann. Bot.*, *95*, 549–567.
Monteith, J. L. (1965), Evaporation and environment, in *Symposium of the Society for Experimental Biology, The State and Movement of Water in Living Organisms*, vol. 19, edited by G. E. Fogg, pp. 205–234, Academic, N. Y.
Mueller, B., et al. (2013), Benchmark products for land evapotranspiration: LandFlux-EVAL multi-dataset synthesis, *Hydrol. Earth Syst. Sci.*, *17*, 3707–3720, doi:10.5194/hess-17-3707-2013.
Nakai, T., and K. Shimoyama (2012), Ultrasonic anemometer angle of attack errors under turbulent conditions, *Agric. For. Meteorol.*, *162–163*, 14–26, doi:10.1016/j.agrformet.2012.04.004.
Nobuhiro, T., A. Shimizu, N. Kabeya, Y. Tsuboyama, T. Kubota, T. Abe, M. Araki, K. Tamai, S. Chann, and N. Keth (2007), Year-round observation of evapotranspiration in an evergreen broadleaf forest in Cambodia, in, *Forest Environments in the Mekong River Basin*, edited by H. Sawada, pp. 75–86, Springer, Tokyo.
Noormets, A., J. Chen, and T. R. Crow (2007), Age-dependent changes in ecosystem carbon fluxes in managed forests in northern Wisconsin, USA, *Ecosystems*, *10*, 187–203.
Pinker R. T., O. E. Thompson, and T. F. Eck (1980), The energy balance of a tropical evergreen forest, *J. Appl. Meteorol.*, *19*, 1341–1350.
Qiu, J. (2009), Where the rubber meets the garden, *Nature*, *457*, 246–247.
Raj, S., G. Das, J. Pothen, and S. K. Dey (2005), Relationship between latex yield of *Hevea brasiliensis* and antecedent environmental parameters, *Int. J. Biometeorol.*, *49*, 189–196.
Rantala, L. (2006), Rubber plantation performance in the Northeast and East of Thailand in relation to environmental conditions, MSc thesis, Dep. of For. Ecol., Univ. of Helsinki, Finland.
Ryu, Y., O. Sonnentag, T. Nelson, R. Vargas, H. Kobayashi, R. Wenk, and D. D. Baldocchi (2010), How to quantify tree leaf area index in a heterogeneous savanna ecosystem: A multi-instrument and multi-model approach, *Agric. For. Meteorol.*, *150*, 63–76, doi:10.1016/j.agrformet.2010.01.009.

San José, J., R. Montes, J. Grace, N. Nikonova, and A. Osío (2008), Land-use changes alter radiative energy and water vapor fluxes of a tall-grass *Andropogon* field and a savanna-woodland continuum in the Orinoco lowlands, *Tree Physiol.*, *28*, 425–435.

Shi, X., J. Mao, P. E. Thonton, and M. Huang (2013), Spatiotemporal patterns of evapotranspiration in response to multiple environmental factors simulated by the Community Land Model, *Environ. Res. Lett.*, *8*, 024012, doi:10.1088/1748-9326/8/2/024012.

Sterling, S. M., A. Ducharne, and J. Polcher (2013), The impact of global land-cover change on the terrestrial water cycle, *Nat. Clim. Change*, *3*, 385–390, doi:10.1038/nclimate1690.

Tan Z.-H., et al. (2011), Rubber plantations act as water pumps in tropical China, *Geophys. Res. Lett.*, *38*, L24406, doi:10.1029/2011GL050006.

Tanaka N., T. Kume, N. Yoshifuji, K. Tanaka, H. Takizawa, K. Shiraki, C. Tantasirin, N. Tangtham, and M. Suzuki (2008), A review of evapotranspiration estimates from tropical forests in Thailand and adjacent regions, *Agric. For. Meteorol.*, *148*, 807–819, doi:10.1016/j.agrformet.2008.01.011.

Tanaka, K., H. Takizawa, N. Tanaka, I. Kosaka, N. Yoshifuji, C. Tantasirin, S. Piman, M. Suzuki, and N. Tangtham (2003), Transpiration peak over a hill evergreen forest in northern Thailand in the late dry season: Assessing the seasonal changes in evapotranspiration using a multilayer model, *J. Geophys. Res.*, *108*(D17), 4533, doi:10.1029/2002JD003028.

Toda, M., K. Nishida, N. Ohte, M. Tani, and K. Mushiake (2002), Observations of energy fluxes and evapotranspiration over terrestrial complex land covers in the tropical monsoon environment, *J. Met. Soc. Jpn.*, *80*, 465–484.

Twine, T. E., W. P. Kustas, J. M. Norman, D. R. Cook, P. R. Houser, T. P. Meyers, J. H. Prueger, P. J. Starkds, and M. L. Wesely (2000), Correcting eddy-covariance flux underestimates over a grassland, *Agric. For. Meteorol.*, *103*, 279–300.

van Dijk, A. I. J. M., and R. J. Keenan (2007), Planted forests and water in perspective, *For. Ecol. Manage.*, *251*, 1–9.

Warren-Thomas, E., P. M. Dolman, and D. P. Edwards (2015), Increasing demand for natural rubber necessitates a robust sustainability initiative to mitigate impacts on tropical biodiversity, *Conserv. Lett.*, *8*, 230–241, doi:10.1111/conl.12170.

Wilson, K., A. Goldstein, E. Falge, M. Aubinet, and D. Baldocchi (2002), Energy balance closure at FLUXNET sites, *Agric. For. Meteorol.*, *113*, 223–243.

Wohl, E., et al. (2012), A research vision for hydrology of the humid tropics: Balancing water, energy, and land use, *Nat. Clim. Change*, *2*, 655–662, doi:10.1038/nclimate1556.

Zhang, L., F. F. Zhao, and A. E. Brown (2012), Predicting effects of plantation expansion on streamflow regime for catchments in Australia, *Hydrol. Earth Syst. Sci.*, *16*, 2109–2121.

Ziegler, A. D., J. M. Fox, and J. Xu (2009a), The rubber juggernaut, *Science*, *324*, 1024–1025.

Ziegler, A. D., T. B. Bruun, M. Guardiola-Claramonte, T. W. Giambelluca, D. Lawrence, T. L. Nguyen (2009b), Environmental consequences of the demise in Swidden agriculture in SE Asia: Hydrology and geomorphology, *Hum. Ecol.*, *37*, 361–373.

Ziegler, A. D., J. M. Fox, E. L. Webb, C. Padoch, S. Leisz, R. A. Cramb, O. Mertz, T. T. Bruun, and T. D. Vien (2011), Rapid land use changes and the role of Swiddening in SE Asia, *Conserv. Biol.*, *25*, 846–848.

Ziegler, A. D., et al. (2012), Carbon outcomes of major land-cover transitions in SE Asia: Great uncertainties and REDD+ policy implications, *Global Change Biol.*, *18*, 3087–3099, doi:10.1111/j.1365-2486.2012.02747.x.